JCTC Journal of Chemical Theory and Computation

pubs.acs.org/JCTC Article

Interaction of Camptothecin with Model Cellular Membranes

Phu K. Tang, Kaushik Chakraborty,[⊥] William Hu,[⊥] Myungshim Kang, and Sharon M. Loverde*

Cite This: https://dx.doi.org/10.1021/acs.jctc.9b00541 Read Online

ACCESS | Metrics & More | Article Recommendations | Supporting Information

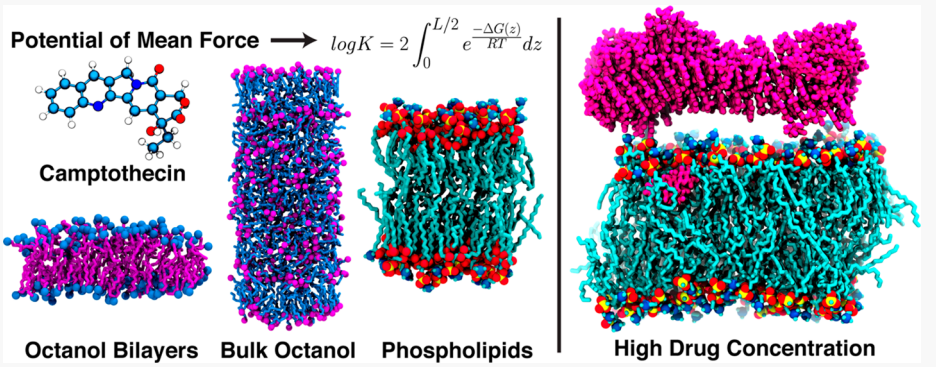

ABSTRACT: Accurate and efficient prediction of drug partitioning in model membranes is of significant interest to the pharmaceutical industry. Herein, we utilize advanced sampling methods, specifically, the adaptive biasing force methodology to calculate the potential of mean force for a model hydrophobic anticancer drug, camptothecin (CPT), across three model interfaces. We consider an octanol bilayer, a thick octanol/water interface, and a model 1-palmitoyl-2-oleoyl-*sn*-glycero-3-phosphocholine (POPC)/water interface. We characterize the enthalpic and entropic contributions of the drug to the potential of mean force. We show that the rotational entropy of the drug is inversely related to the probability of hydrogen bond formation of the drug with the POPC membrane. In addition, in long-time microsecond simulations of a high concentration of CPT above the POPC membrane, we show that strong drug−drug aromatic interactions shift the spatial orientation of the drug with the membrane. Stacks of hydrophobic drugs form, allowing penetration of the drug just under the POPC head groups. These results imply that inhomogeneous membrane models need to take into account the effect of drug aggregation on the membrane environment.

1. INTRODUCTION

Biopharmaceutical investments cost about $90 billion, surpassing other industrial investments in 2016.[1] However, phase I,[2] II,[3] and III[4] trials are mostly limited because of the poor bioavailability and efficacy of current R&D models.[5] Knowing how to fine-tune permeability of small compounds across the membrane is of significant interest to the pharmaceutical industry. Over one century ago, Overton's rule[6] first established a quantitative relationship between membrane permeability and the partition coefficient of small compounds. Using the 1-octanol (octanol) partition coefficient in pharmacology is an efficient means to quickly predict the permeability of hundreds of small molecular compounds. Indeed, this becomes a daily routine in most drug discovery laboratories. Quantitative structure−property relationship (QSPR) models,[7] as well as quantitative structure−activity relationship (QSAR) models,[8] have also proved their potential as quantitative methods to assess the permeability of small molecules based on their physiochemical properties such as oral bioavailability,[9] intestinal absorption,[10] as well as ability to cross the blood-brain barrier.[11] Notably, there has been an increasing interest in the computational chemistry field to harness the power of statistical methods, such as machine learning approaches, to predict small drug permeability in membranes.[12−14]

At the simplest level a membrane can be considered a homogeneous slab, where the permeability of a solute through the membrane is inversely proportional to the thickness of the membrane. The membrane permeability, P, can be expressed in terms of the bulk properties, such that $P = \frac{KD}{2L}$, where D is the diffusion coefficient of the solute in the membrane, K is membrane/water partition coefficient, and $2L$ is the thickness of the membrane.[15,16] However, the solute, or drug, can possess multiple degrees of freedom. The effect of the drug conformation on the free energy profile across a membrane interface can be explored with advanced sampling methods in molecular dynamics.[17] Likewise, the solubility-diffusion model

Received: June 3, 2019
Published: March 3, 2020

https://dx.doi.org/10.1021/acs.jctc.9b00541
J. Chem. Theory Comput. XXXX, XXX, XXX−XXX

can be expanded in terms of the translational and rotational degrees of freedom of the solute.[15,18] Furthermore, inhomogeneous membrane models that consider variation of phospholipid composition in realistic membranes must also be considered.[19−21]

With the increase in current state-of-art computational power, molecular dynamics (MD) simulations offer a powerful tool to probe the multitudes of length-scales[22,23] and time-scales,[24−26] especially in biological phenomena such as membrane permeability and transport across membrane interfaces. In particular, enhanced sampling methods in molecular dynamics offer emerging and powerful tools to probe the membrane permeability of small molecular compounds.[17,27−32] Several enhanced sampling methods that can characterize the free energy profile across the membrane interface are thermodynamic integration,[33,34] metadynamics,[35−38] umbrella sampling,[39] and the adaptive biasing forces (ABF) method.[31,40−43] In the ABF method, an on-the-fly force to counter the internal system force is continuously updated, requiring no a-priori knowledge of the free energy profile.

Camptothecin[44] (CPT), a model hydrophobic anticancer drug, is a topoisomerase I inhibitor.[45,46] CPT possesses a planar pentacyclic ring structure. A molecular diagram of CPT is included in Supporting Figure 1. Notably, the pK_a of the hydroxyl oxygen is 11.69, thus the hydroxyl oxygen will remain deprotonated across the interfaces, unless there are significant shifts in the pK_a value.[47] A unique property of CPT is that it is known to self-assemble in solution into filamentous assemblies.[48,49] Herein, we characterize in the free energy profile of this model hydrophobic anticancer drug, CPT, across three model interfaces of varying thickness: an octanol bilayer/water interface (∼20 Å) (interface I), a thick octanol slab/water interface (∼80 Å) (interface II), and a model phospholipid bilayer membrane composed by 1-palmitoyl-2-oleoyl-*sn*-glycero-3-phosphocholine (POPC)/water interface (∼40 Å) (interface III). Together with hydrogen bonds, rotational angle of the drug, as well as drug enthalpy, we characterize the interaction of this model hydrophobic drug with these three model interfaces using advanced sampling methods, specifically the ABF method. Moreover, on the basis of the Schlitter method,[50−52] we also characterize the rotational entropy of the drug across each model interface. The Schlitter method estimates the upper value of configurational entropy by diagonalizing the covariance matrix of the Cartesian positional fluctuations of atoms obtained from MD simulation. Here, we apply a modified version of this method, described in further detail in the methods section, to characterize the rotational entropy of the hydrophobic cancer drug, CPT. We next suggest that the strength of hydrogen bonding of this model drug with a model phospholipid bilayer is inversely correlated with the rotational entropy of the drug. Finally, we show that CPT can form strong aromatic interactions with itself at high concentrations above this model phospholipid bilayer. The strong aromatic interactions lead to the formation of stacks of drug above the membrane interface, modulating the interaction of the drug with the phospholipid bilayer. This shift allows penetration of the drug just under the POPC head groups. We suggest that this mechanism of membrane permeation may apply to other hydrophobic compounds with strong aromatic interactions.

2. METHODS

2.1. Simulation Setup. *2.1.1. Bilayer of 1-Octanol (Interface I).* A 20-Å bilayer (Figure 1) of 1-octanol was

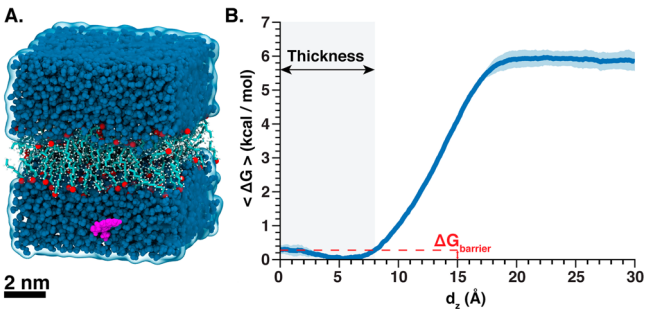

Figure 1. (A) Interface I: A snapshot of the octanol bilayer and CPT interface. The oxygen atoms are highlighted in red and the CPT is shown in magenta licorice representation. Waters are shown in blue. (B) The PMF profile, Δ*G*, in kcal/mol, of transferring the CPT along the *z*-direction of the octanol bilayer averaging over three separate replicas, where d_z is the distance from the center of mass of the octanol bilayer in ångstroms. Error bars (based on the 95% confidence interval) are shown in light blue. The shaded area indicates the thickness of the bilayer based on electron density.

preassembled using Packmol.[53] The 1-octanol was parametrized using CHARMM36.[54−57] The hydrophobic cancer drug CPT was based on the General Automated Atomic Model Parameterization (GAAMP) method developed by Huang and Roux.[58] This automated parametrization server optimizes electrostatic potential and "soft" dihedrals (conformational changes) via quantum mechanical results (as used in AMBER) and water interactions (as used in CHARMM). Overall, this system contained 20 350 atoms, which included 200 1-octanols, 4954 TIP3P waters; and one CPT molecule placed 35 Å above the center of mass (COM) of the octanol bilayer. Additionally, 150 mM of NaCl was added to the simulation box. The final box, after 40 ns of equilibration, was 56 Å × 56 Å × 65 Å.

2.1.2. Thick 1-Octanol Layer (Interface II). A layer of 1-octanol with the thickness of 100 Å (Figure 2) was preassembled using Packmol.[53] The 1-octanol and the CPT parameters were the same as interface I. Overall, this system contained 31 719 atoms, which included 620 1-octanols and 4963 TIP3P waters. We set up the initial concentration of ∼0.26 mole fraction of water; however, after ∼80 ns, the system equilibrated with a mole fraction of ∼0.23. The system reached stable dimensions of 46 Å × 38 Å × 172 Å. In addition, 150 mM NaCl was added to the simulation box. One CPT was placed at the center of mass (COM) of the bulk octanol.

2.1.3. Model Phospholipid Bilayer (Interface III). A pure 1-palmitoyl-2-oleoyl-*sn*-glycero-3-phosphocholine (POPC) membrane bilayer (Figure 3) was setup using Packmol.[53] The CHARMM36 membrane force field was used for POPC.[55] The CPT parameters were the same for interface I and II. In total, the membrane bilayer system contained 23 782 atoms, which contained 59 POPCs and 5268 TIP3P waters. Also, 150 mM of NaCl was added to the system. The area per lipid was approximately 59.9 ± 1.8 Å^2, and its thickness was approximately 40 Å at 310 K. The area per lipid was calculated with a block averaging approach with 9 blocks of 1.9 ns. These characteristics agree well with experimental measurements for

https://dx.doi.org/10.1021/acs.jctc.9b00541
J. Chem. Theory Comput. XXXX, XXX, XXX−XXX

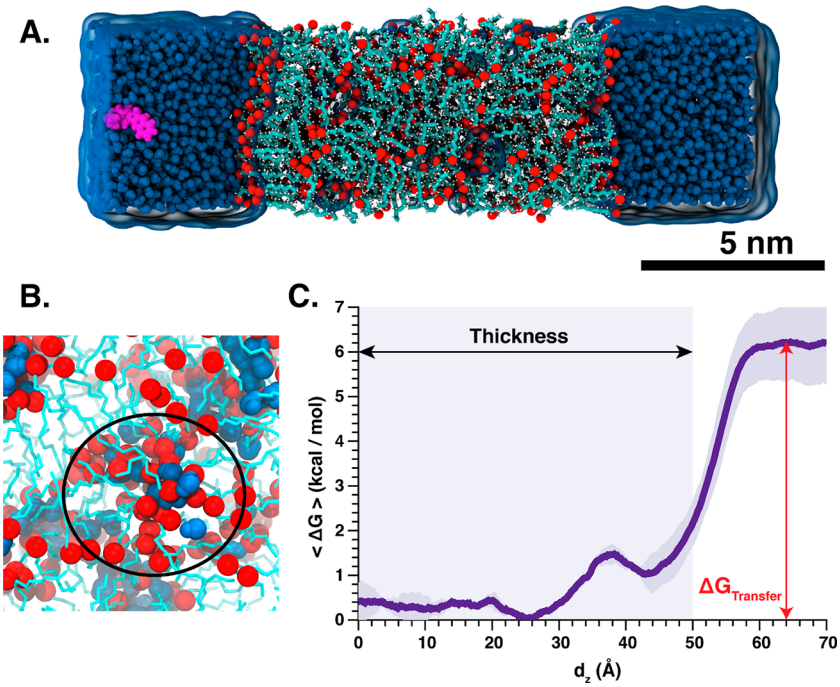

Figure 2. (A) Interface II: A snapshot of the octanol layer and CPT (in magenta) placed about 70 Å away from the center of mass of the octanols. Notice the hydrophilic paths that are created from the hydroxyl groups and some waters are found inside those paths. (B) A snapshot shows the "overlapping elongated inverse micelles" region (circled). (C) The PMF of the CPT along the *z*-direction of the octanol bilayers after 60 ns. Error bars (based on the 95% confidence interval) are shown in light purple. The electron density shows the thickness of the bulk octanol layer. The shaded area indicates the thickness of the bilayers based on its electron density.

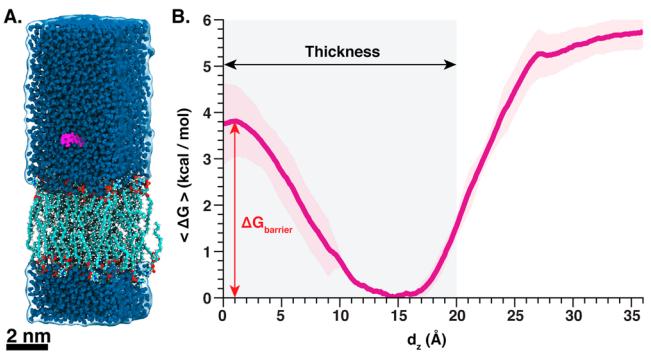

Figure 3. (A) Interface III: A snapshot of the POPC membrane bilayer and CPT (in magenta). (B) The PMF profile, Δ*G*, in kcal/mol, of transferring the CPT along the *z*-direction of the POPC bilayer averaged over two replicas, where d_z is the distance from the center of mass of the POPC bilayer in Angstroms. Error bars (based on the 95% confidence interval) are shown in light pink. The shaded area indicates the thickness of the bilayer based on electron density.

POPC bilayer.[59] Our simulations are at 310 K, far above the gel transition temperature for POPC, which is 271 K. After 80 ns of equilibration, the box dimensions were stable at 43 Å × 40 Å × 133 Å. One molecule of CPT was placed 35 Å above the COM of the POPC bilayer membrane.

2.1.4. High CPT Concentration. The system contained 84 CPT molecules, 163 POPCs, 13 097 TIP3P waters, and 37 NaCl molecules. In total, the system had 65,743 atoms. The box dimensions were 92 Å × 92 Å × 125 Å. The simulation time was 1.6 μs, at 310 K with anisotropic pressure. The bilayer thickness was approximately 40 Å at 310 K.

2.2. MD Simulation Parameters. *2.2.1. Simulation Parameters.* All MD simulations were carried out using NAMD2[60] version 2.12b. Interface I used an isotropic NPT ensemble; interface II used an NPAT ensemble, and interface III used an anisotropic NPT ensemble with fixed x/y ratio. A temperature of 298 K was used for the octanol–water systems (interface I and II) and a temperature of 310 K was used for the membrane bilayer (interface III). A damping coefficient of $\gamma = 1$ ps^{-1}, at a pressure of 1 atm, was used together with the Langevin piston Nosé–Hoover method[61,62] for the octanol–water systems. The Langevin piston Nosé–Hoover method in NAMD is a combination of the MTK constant pressure algorithm[61] with Langevin dynamics for piston fluctuation control.[62] However, the membrane bilayer used an anisotropic piston to allow realistic fluctuations of the membrane. A piston period of 200 fs and a damping time scale of 50 fs were used in all systems. The SHAKE algorithm[63] was used to fix hydrogen atoms allowing a 2 fs time step. The particle mesh Ewald (PME) algorithm[64] was utilized to take full electrostatic interactions into account, with full periodic boundary conditions. The cutoff for van der Waals interactions was 12 Å with a smooth switching function at 10 Å used to truncate the van der Waals potential energy at the cutoff distance. Bonded atoms were excluded from nonbonded atom interactions using a scaled 1–4 value. Coordinates were saved every 2 ps for analysis. A summary of MD configuration parameters is shown in Table 1.

2.2.2. Free Energy Calculations. The converged free energy profiles, or the potential of mean force (PMF), across the three model interfaces were calculated using the adaptive biasing force or the ABF method.[31,40–43] In ABF calculations, an external force is continuously estimated and imposed along the chosen reaction coordinates, ξ^*, to cancel out the total average of the acting mean force on the system

https://dx.doi.org/10.1021/acs.jctc.9b00541
J. Chem. Theory Comput. XXXX, XXX, XXX–XXX

Table 1. Summary of Initial Set-up of ABF Configurations for All Interfaces

system	octanol bilayer (interface I)	thick octanol layer (interface II)	POPC membrane bilayer (interface III)
Box dimensions (Å)	56 × 56 × 65	46 × 38 × 175	43 × 40 × 133
atoms	20 350	31 719	23 782
water (molecules)	4954	4967	5268
other (molecules)	200 octanols	620 octanols	59 POPCs
number of replicas	3	2	2
temperature (K)	298	298	310
pressure	isotropic	anisotropic	anisotropic
constant area	N/A	yes	partially (constant ratio)
window width (Å)	2	2	3
number of windows	15	35	12
distance (d_z) (Å)	30	75	36
total run time (ns)	35 (rep1) and 40 (rep2,3)	60 (rep1,2)	142 (rep1) and 145 (rep2)
mole fraction of water	0	~0.23	0

$$\langle F_\xi|\xi^*\rangle = -\frac{A}{d\xi}(\xi^*)$$

Here, F_ξ is the total acting force, and A is the free energy along ξ^*. The standard deviation in the PMF profiles, SD$[\Delta A^{(abf)}]$, were approximated using the method by Rodriguez-Gomez et. al,[65] where κ is the correlation length,[66] $\xi_b - \xi_a$ is the width of each window or bin, σ^2 is variance$[F_\xi]$, and K is the number of steps

$$\mathrm{SD}[\Delta A^{(abf)}] \approx (\xi_b - \xi_a)\frac{\sigma}{K^{1/2}}(1 + 2\kappa)^{1/2}$$

To increase the efficiency the reaction coordinate, ξ, was truncated into smaller distances, $(\xi_b - \xi_a)$. The octanol bilayer, bulk octanol, and membrane bilayer were divided evenly into 15, 35, and 12 windows with the widths of 2, 3.5, and 3 Å, respectively. The initial configurations of each window were selected from trajectories obtained from steered molecular dynamics (SMD) simulations.[67] During SMD simulations, a harmonic constraint was placed on the COM of the POPC phospholipid bilayer with a spring constant of 50.0 kcal/mol/Å^2 to minimize upward and downward motion of the bilayer throughout the trajectory. Three replicas of the PMF were calculated across an octanol bilayer/water interface (interface I), two replicas of the PMF were calculated across a thick octanol slab/water interface (interface II), and two replicas of the PMF were calculated across a model phospholipid bilayer membrane (POPC/water) interface (interface III). The first replica of each of the free energy profiles of the CPT with the octanol bilayer, bulk octanol, and membrane bilayer were converged after 35, 60, and 142 ns, respectively. A summary of system setup and sizes are in Table 1.

2.2.3. Orientation Angle. The angle θ between the CPT and the interface in question was calculated using

$$\vec{A}\cdot\vec{z} = \cos\theta\cdot|\vec{A}|\cdot|\vec{z}|$$

Here, θ is the angle between the vector $\vec{A}$ on CPT, which was defined by **C16−O2** (numbering was solely based on PDB, see Supporting Figure 2), and the unit vector $\vec{z}$ of the box. All physical fluctuations of the bilayer or the thick octanol were disregarded to simplify the angle calculations.

2.2.4. Partition Coefficient. The partition coefficient was calculated with two different methodologies. The first method of calculating the partition coefficient, log P, of CPT in each system was extrapolated using the free energy profile from ABF calculation

$$\log P = \frac{-\Delta G^{w\to o}_{transfer}}{RT\ln(10)} = \frac{-(\Delta G_{octanol} - \Delta G_{water})}{RT\ln(10)} = \frac{\Delta G_{water} - \Delta G_{octanol}}{RT\ln(10)}$$

where R is the gas constant and T is the temperature. In the second method, the partition coefficient of CPT in each system was calculated from

$$K = 2\int_{L/2}^{0} e^{-\Delta G(z)/RT}\,\mathrm{d}z$$

where L is the width of the interface.[68] Here, log P is the same as log K.

2.2.5. Rotational Entropy. The rotational entropy of the CPT drug is estimated from the principal root-mean-square (rms) fluctuations of Euler angles. We utilize the method from Carlsson and Aqvist et al.[69] Rotational entropy of any molecule can be written as

$$S^{rot} = -\frac{R}{h^3}\int \mathbf{p}(p, r)\ln(p, r)\,\mathrm{d}p\,dr$$

where $\mathbf{p}(p, r)$ is the position and momentum in rotational phase space. The above equation can also be written as

$$S^{rot} = R\ln\left[\frac{1}{\sigma_s}\left(\frac{2\pi e k_B T}{h^2}\right)^{3/2}(I_a I_b I_c)^{1/2}\right] - R\int P_{rot}(\Theta)\ln P_{rot}(\Theta)\mathrm{d}\Theta$$

where R is the gas constant, k_B is Boltzmann's constant, e is Euler's number, T is the temperature, σ_s is the symmetry number, I_a, I_b, I_c are the time average moment of inertia along the three principal axis, and $P_{rot}(\Theta)$ is the probability density of positions in rotational phase space. It is very difficult to obtain the correct $P_{rot}(\Theta)$ from molecular dynamics simulation trajectories, especially for complex systems. Thus, we use a Gaussian distribution to calculate $P_{rot}(\Theta)$.[52] The Gaussian probability distribution can be written as $P_{rot}(\Theta) = \frac{1}{(2\pi)^{3/2}\det(\sigma)^{1/2}}\exp\left[-\frac{1}{2}(\chi - \overline{\chi})\sigma^{-1}(\chi - \overline{\chi})\right]$, where χ is the rotational variable (the Euler angles) and σ is the covariance matrix of the Euler angles. Finally, the rotational entropy can be written as[51,69]

$$S^{rot,gaussian} = R\ln\left[\frac{(2\pi e)^{3/2}}{\sigma_s}\left(\frac{2\pi e k_b T}{h^2}\right)^{3/2}\times(I_a I_b I_c)^{1/2}\sigma_\phi\sigma_\psi\sigma_\theta\sin\overline{\theta}\right]$$

where R is the gas constant, e is the Euler number, σ_s is the symmetry number, which normalizes the number of different molecular conformations by rotation,[70] k_b is the Boltzmann's constant, h is the Planck's constant; I_a, I_b, I_c are the principal moments of inertia, and $\overline{\theta}$ is the average value for θ from $0 \le \theta$

https://dx.doi.org/10.1021/acs.jctc.9b00541
J. Chem. Theory Comput. XXXX, XXX, XXX−XXX

$\leq \pi$. Here, $0 \leq \varphi \leq 2\pi$, $0 \leq \psi \leq 2\pi$, and $0 \leq \theta \leq \pi$ are the Euler angles. The formula includes deformation of the drug structure accounted for in the principal moments of inertia.

2.2.6. Drug Enthalpy. The average drug enthalpy, ΔH_{drug} for each window was calculated as

$$H_{drug} = E_{van\ der\ Waals} + E_{electrostatics}$$

For H_{drug}, we include the interactions between CPT and its surrounding species, such as CPT−water, CPT−POPC, CPT−octanol, and CPT−ion. All other interactions between non-CPT molecules were excluded. These interactions between non-CPT molecules should be included in the total enthalpy $H_{total} = H_{drug} + H_{environment}$, where $H_{environment}$ includes the surrounding molecules, such as phospholipid, the octanol, and water.

2.2.7. Hydrogen Bonds. The hydrogen bond analysis was performed using the Cpptraj package[71] from AmberTools. The cutoff angle was 120°, and the cutoff distance was 3 Å. Since CPT and octanol can both be hydrogen donor and acceptor, we consider both cases. The atoms used to calculate the H bonds are the oxygen from the hydroxyl on the CPT, the oxygen from the hydroxyl on the octanol, and either the oxygen from the phosphate or nitrogen from the choline group on the POPC.

3. RESULTS AND DISCUSSION

In the present work, we characterize the free energy profiles of a model hydrophobic anticancer drug, CPT, across three different interfaces—an octanol bilayer/water interface (interface I), a thick octanol slab/water interface (interface II), and a model phospholipid bilayer membrane composed by 1-palmitoyl-2-oleoyl-*sn*-glycero-3-phosphocholine (POPC)/water interface (interface III)—using the ABF methodology. We next characterize the enthalpic and entropic energetic contributions of CPT with these three interfaces (interfaces I, II, and III).

3.1. Calculation of Free Energy Profiles. To begin with, we calculate the potential of mean force profile, ΔG, in kcal/mol, across three replicas of interface I. As shown in Figure 1A, the octanol bilayer exhibits significant fluctuations, but the octanol is still fairly ordered at the interface. Moreover, the octanol bilayer is significantly thinner (∼20 Å) than a model phospholipid membrane bilayer (∼40 Å). See Supporting Figure 3, for a snapshot of the system setup and the electron density. To address the convergence of the free energy profiles, we show the time evolution of the first replica of the free energy profile, the variations in the gradient forces, as well as the total counts in Supporting Figure 4. The $\Delta G_{transfer}$, as indicated in Figure 1 B, calculated is 5.5 kcal/mol. At the hydrophobic center of the octanol bilayer, CPT experiences a very small energy barrier, $\Delta G_{barrier}$, 0.5 kcal/mol. The corresponded partition coefficient, log P, was calculated from the $\Delta G_{transfer}$ to be 4.0. The second method of calculating the partition coefficient, from $\int e^{PMF/RT}$ gives log K = 1.8. In comparison, the octanol/water partition coefficient of CPT is known to be 1.74.[72] The second method, integrating the values of the local partition coefficients across the interface, gives very close agreement with experimentally reported results, even though we are simulating a very thin octanol bilayer.

Next, we construct a thick layer of octanol (∼80 Å) to characterize the effect of increased thickness on the free energy profile across interface II. We calculate the potential of mean force profile, ΔG, in kcal/mol, across two replicas of this interface. We start the free energy calculation at the COM of the bulk octanol layer. The octanol slab exhibits tail and head enriched regions; which are scattered throughout the bulk octanol layer (see Figure 2A), first described as "overlapping elongated inverse micelle" regions by Tieleman et al.[73] (see Figure 2B). The hydroxyl groups line up to form hydrophilic paths so that water molecules penetrate the bulk phase from both sides of the octanol layer. According to the electron density profile (see Figure 2C), at ∼55 Å away from the COM of the octanol, we see the effects of the neighboring bulk water on the ordering of the octanol at the interface, with the 1-octanol at the surface forming an ordered monolayer. To address the convergence of the free energy profiles, we show the time evolution of the first replica of the free energy profile, the variations in the gradient forces, as well as the total counts in Supporting Figure 5. After 60 ns, the PMF profile converges. We calculate the potential of mean force profile, ΔG, in kcal/mol, across three replicas of the thick octanol interface (Figure 2C). The $\Delta G_{transfer}$ calculated at 70 Å from the COM of the slab with a value of 6.2 kcal/mol. This corresponds to an overestimated partition coefficient of 4.6. The second method of calculating the partition coefficient, from $\int e^{PMF/RT}$ gives log K = 2.2; however, it is much closer to the experimentally reported partition coefficient of 1.74.[72] We note that the ordering of the 1-octanol across the interface corresponds to multiple barriers within the free energy profile. Here, the influence of the thickness of the octanol layer plays multiple roles. To begin with, the interface is wider by a factor of 4. Moreover, the ordering of the octanol across the interface in both cases, the octanol bilayer as well as the thick octanol layer, is substantially different.

We next calculate the potential of mean force profile, ΔG, in kcal/mol, across two replicas of the POPC bilayer/water interface (Figure 3 B). The CPT was initially placed 35 Å away from the COM of a model POPC phospholipid membrane bilayer (see Figure 3A). See also Supporting Figure 6 for additional snapshots of the system setup and electron density. We show the time evolution of the first replica of the free energy profile, the variations in the gradient forces, as well as the total counts in Supporting Figure 7. In addition, the time dependent violin plot of the orientation angles for both replicas are shown in Supporting Figures 8 and 9. The free energy to transfer CPT across interface III is found to be 5.8 kcal/mol (see Figure 3B) after nearly 166 ns ABF calculations. From the $\Delta G_{transfer}$, the partition coefficient was calculated to be 4.05. To our knowledge, there is no available experimental partition coefficient for CPT with POPC. However, a value of 1.67 was reported with DOPC.[74] The second method of calculating the partition coefficient, from $\int e^{PMF/RT}$ gives log K = 1.9. This is a difference of 13% from the reported value for the partition coefficient with DOPC, which seems reasonable. The barrier free energy for CPT to cross the hydrophobic core from one leaflet to another is approximately 3 kcal/mol. To summarize, here, we calculate the partition coefficient for a model hydrophobic drug across three different model hydrophobic interfaces with increasing degrees of thickness and heterogeneities in composition. Slow convergence of the free energy profiles, in particular across the model POPC phospholipid bilayer suggest multiple hidden reaction coordinates.

3.2. Spatial Orientation of Drug. To characterize one of the first most probable hidden reaction coordinates, we characterize the spatial orientation of CPT with respect to the normal vector of the model interfaces, along the reaction

https://dx.doi.org/10.1021/acs.jctc.9b00541
J. Chem. Theory Comput. XXXX, XXX, XXX−XXX

coordinate, d_z. We consider the interfaces to be rigid and neglect vertical fluctuations of the layers. Thus, the calculated angle of the drug reflects its relative orientation to each respective layer.

In Figure 4, violin plots show the distribution of angles between the three interfaces and CPT. In Figure 4A, for the

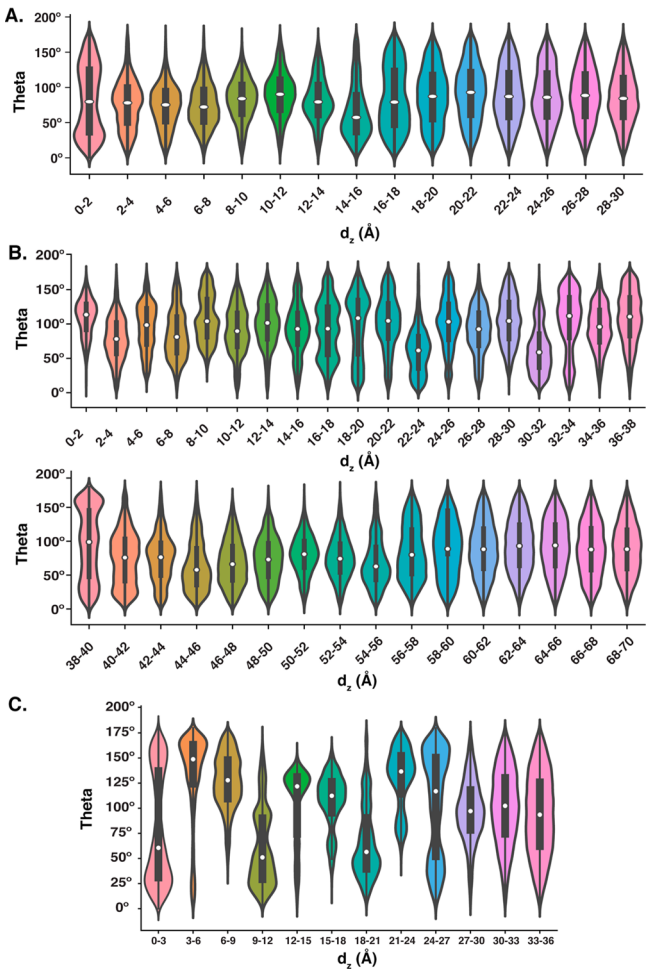

Figure 4. (A) Violin plots showing the distribution of θ angles between CPT and the normal vector of the octanol bilayer (interface I) for the first replica. Each plot is calculated on each window. The white dots are averaged angles. The black bars indicate the 95% confidence interval. (B) Violin plots showing the distribution of θ angles between CPT and the normal vector of the thick octanol (interface II) for the first replica. Each plot is calculated on each window. The white dots are averaged angles. The black bars indicate the 95% confidence interval. (C) Violin plots showing the distribution of θ angles between CPT and the normal vector of the POPC bilayer (interface III) for the first replica. Each plot is calculated on each window. The white dots are average angles. The black bars indicate the 95% confidence interval.

octanol bilayer (interface I) CPT is slightly tilted parallel to the acyl chains as shown by higher population of angles around 25° and 130°. Most likely, this is to minimize the local steric hindrances within the hydrophobic core. However, when CPT is in the interfacial region, approximately from 5 Å away from the COM of the octanol bilayer, interactions between the CPT and the octanol bilayer, such as hydrogen bonds, shifts the distribution of the angles to around 80−110°. This implies that the CPT is almost parallel to the octanol bilayer, with the only hydroxyl group of the CPT pointing toward the hydroxyl groups of the octanols. In Figure 4B, for the thick octanol layer (interface II), the distribution of angles is quite different from the ordered octanol bilayer. As expected, the "overlapping elongated inverse micelles" influence the orientation of CPT. Until about 40 Å away from the COM, CPT rotates freely. However, at 42−46 and 60−63 Å, there are strong interactions that correspond to minima in the PMF (see Figure 2B).

The distribution of angles of CPT with respect to the phospholipid membrane bilayer (interface III) suggests strong interactions of the CPT with the phospholipids in the interfacial region (see Figure 4C). Compared to the other two systems, the POPC head groups have more pronounced effects on the orientation of the CPT. CPT is slightly tilted parallel to the acyl chains in the center of the membrane indicated by the higher population of angles around 25° and 150°, with a distinct lack of CPT oriented at an angle of 90°. However, we find that CPT can make a nearly 180° flip as a rare event in the simulation trajectory. Indeed, the strong orientational dependence of the CPT in the membrane causes slow convergence of the PMF profile in this region (see Figure 3B). It is possible that spatial orientation can be used as the second reaction coordinate for the free energy surface across the phospholipid membrane bilayer in future studies. Figure 4C also demonstrates that within the interfacial region, CPT is not as parallel to the membrane as in the other two model interfaces. Instead, the CPT points its hydroxyl group toward the POPC head groups. Since the POPC is zwitterionic, electrostatic interactions can also play a role. For example, the drug can exhibit multiple electrostatic interactions with the dipole layer of the POPC membrane. Next, we further explore the relationship between the strength of hydrogen bonds between the drug and the interfaces (I, II, and III) and how this affects the rotational entropy of the drug. In addition, we characterize the van der Waals and electrostatic contributions to the enthalpy.

3.3. Hydrogen Bonds, Rotational Entropy, and Enthalpy. Next, from the ABF trajectories, we quantify the average numbers of hydrogen bonds, ⟨H bonds⟩, and the rotational entropy of the CPT, $S_{\text{rotational}}$, for all three interfaces, averaging over the first replica. One should note that both CPT and octanol molecules can be hydrogen bond donors and acceptors. As mentioned above, to be consistent and compare all three systems, CPT and octanols were both analyzed as a donor and acceptor while POPC was only considered as a donor. With the octanol bilayer (interface I), there are two minima of the $S_{\text{rotational}}$ (see Supporting Figure 10) as the CPT approaches the membrane. One of them matches the minimum in the PMF profile, while the other is close to the interfacial region. As shown in Supporting Figure 11, which includes a detailed cross correlation coefficient matrix between the electrostatic energy, H-bonding, the PMF, the rotational entropy, and the van der Waals energy for the thin octanol bilayer, the PMF is very weakly anticorrelated with the rotational entropy. With the thick octanol layer (interface II), H bonds consistently form everywhere, especially in the interfacial region, as well as inside the thick octanol phase. One might suspect that CPT is then locked into a specific spatial orientation. However, the angle analysis and the $S_{\text{rotational}}$ indicate otherwise. CPT rotates freely in the bulk octanol phase (see Figures 4B and 5). Whereas there are three minima in the PMF profile, the $S_{\text{rotational}}$ profile possesses multiple minima with a maximum in the water. We find that the lower

https://dx.doi.org/10.1021/acs.jctc.9b00541
J. Chem. Theory Comput. XXXX, XXX, XXX−XXX

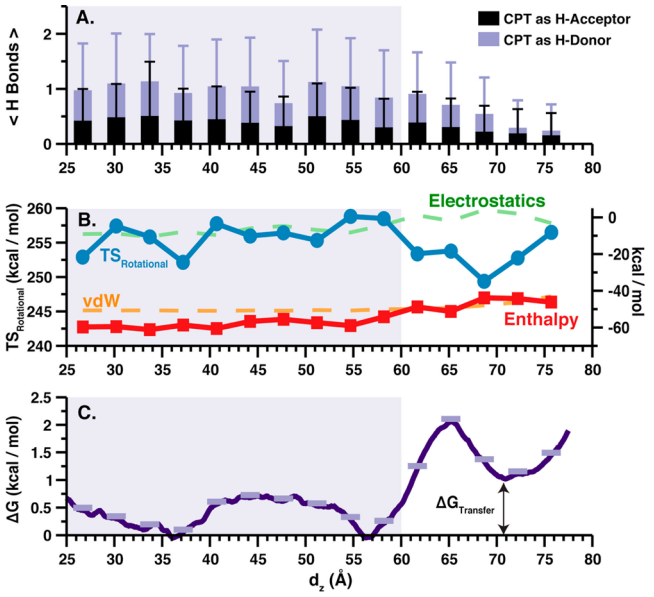

Figure 5. Interface II: (A) The average number of hydrogen bonds for each window of the thick octanol slab in both situations where CPT can be a donor (purple) or acceptor (black). The bars indicate standard deviation. (B) The rotational entropy of CPT ($TS_{rotational}$), the enthalpy, which has contributions due to the van der Waals (vdW), and the electrostatics are plotted along the distance between the center of mass of CPT and the thick octanol slab. The left axis is for the rotational entropy of CPT only. (C) The ΔG in kcal/mol of the CPT along the z-direction of the thick octanol layer after 60 ns. Error bars are in light purple. The shaded area indicates the thickness of the thick octanol layer based on its electron density. All data shown for first replica.

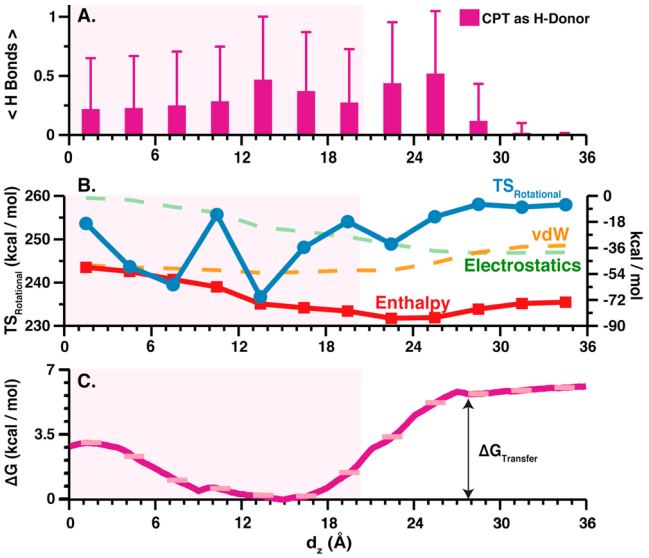

Figure 6. Interface III: (A) The average numbers of hydrogen bonds bonds for each window along the POPC interface in both situations where CPT can be a donor (magenta). The bars indicate standard deviation. (B) The rotational entropy of CPT ($TS_{rotational}$), the enthalpy, which has contributions due to the van der Waals (vdW), and the electrostatics, are plotted along the distance between the center of mass of CPT and the POPC bilayer. The left axis is for the rotational entropy of CPT only. (C) The The ΔG in kcal/mol along the z-direction of the POPC bilayer after 166 ns. Error bars are in light magenta. The shaded area indicates the thickness of the POPC bilayer based on its electron density. All data shown for first replica.

free energy within the thick octanol layer is favorable from electrostatic, enthalpic, and entropic contributions due to the rotational entropy of the drug. As shown in Supporting Figure 12, which includes a detailed cross correlation coefficient matrix between the electrostatic energy, H-bonding, the PMF, the rotational entropy, and the van der Waals energy for the thick octanol bilayer, the PMF is also very weakly anticorrelated with the rotational entropy, which is similar to the thin octanol bilayer.

With the POPC membrane bilayer (interface III), the average number of hydrogen bonds is lower than the other two systems (see Figure 6A). Interestingly, similar to the octanol bilayer, the two minima of $S_{rotational}$ were similar to those in the PMF profile (see Figure 6B and C). Importantly, when the CPT loses its rotational entropy, the average number of hydrogen bonds increases, with the corresponding minima in the PMF. However, in the inner hydrophobic core of the membrane, CPT regains its rotational entropy due to the spontaneous breaking of $C-H_{CPT}\cdots O_{POPC}$ hydrogen bonds. As the CPT crosses the phospholipid membrane interface, the dominant hydrogen bond for each position based on its lifetime is shown in Figure 7. At 6−9 Å the dominant hydrogen bond is $C-H_{CPT}\cdots O_{Glycerol/POPC}$ hydrogen bonds. At 12−15 Å the dominant hydrogen bond is $O-H_{CPT}\cdots O_{Phosphate/POPC}$ hydrogen bonds. At 21−24 Å the dominant hydrogen bond is $O-H_{CPT}\cdots O_{Glycerol/POPC}$ hydrogen bonds. In contrast to the thick octanol layer, we find that the lower free energy within the POPC membrane bilayer is unfavorable from electrostatic and enthalpic contributions; however, the rotational entropy of the drug corresponds with the location of the free energy minimum. Thus, we infer that with more complex and ordered interfaces the rotational entropy of the drug can play a significant role in the location of the free energy minimum. In particular, the rotational entropy of the drug is inversely related to the average numbers of hydrogen bonds of the drug with the phospholipid headgroups. The cross correlation coefficient for the rotational entropy of the drug with respect to the average number of hydrogen bonds is −0.48. A detailed cross correlation coefficient matrix between the electrostatic energy, H-bonding, the PMF, the rotational entropy, and the van der Waals energy for the POPC bilayer is shown in Supporting Figure 13. We calculate the difference in rotational entropy, van der Waals, and electrostatic interactions in the bulk vs the minimum in the POPC bilayer. The relative difference in rotational entropy is 31.0 kcal/mol, while the difference in van der Waals and electrostatic interactions are −18.9 and 17.4 kcal/mol, respectively. Notably, the rotational entropy contribution is nearly twice the van der Waals and electrostatic contributions and is playing a critical role. Thus, at the cost of decreasing rotational entropy, the minimum in the PMF profile is still within the bilayer and the transfer free energy is 5.8 kcal/mol. This suggests that additional environmental contributions to the enthalpy (and entropy) are the determining factors in setting the relative minimum for the drug in the interface and the overall magnitude of the transfer free energy.

4. HIGHER CONCENTRATION OF CPTS

We next hypothesize that the calculated partition coefficient may neglect of cooperative CPT−CPT interactions, as well as how this CPT drug stacking will affect the hydrophobic environment of the membrane.[48,75] To test the degree of

https://dx.doi.org/10.1021/acs.jctc.9b00541
J. Chem. Theory Comput. XXXX, XXX, XXX−XXX

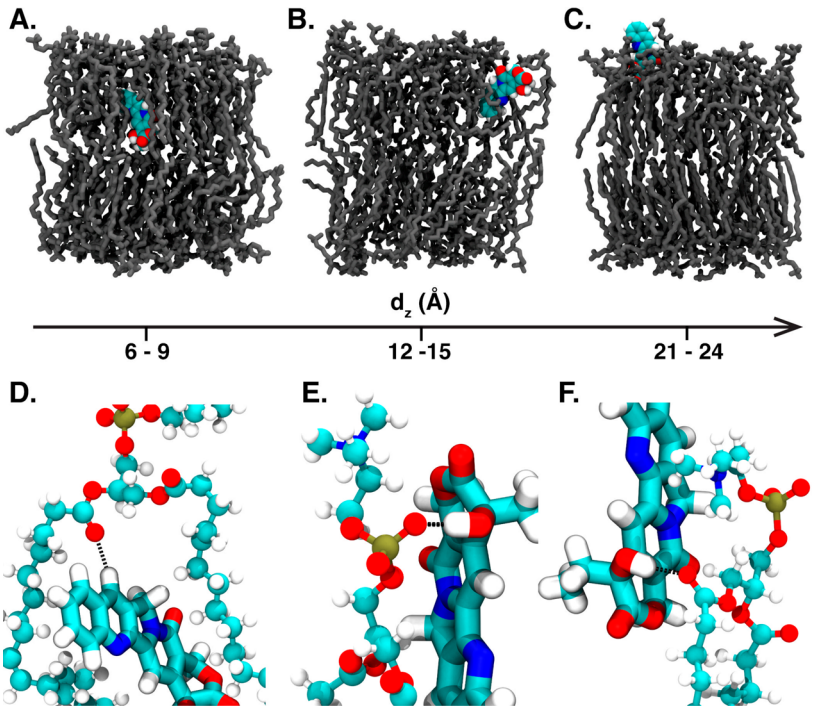

Figure 7. (A−C) Relative position and orientation of CPT with respect to the POPC membrane bilayer (interface III) at a distance of 6−9, 12−15, and 21−24 Å. (D−F) The dominant hydrogen bond at a distance of 6−9, 12−15, and 21−24 Å based on its lifetime.

CPT—CPT stacking and how the stacking will disrupt the membrane interface, we ran a long-time 1.6 μs simulation of multiple CPTs above a slightly larger POPC bilayer at a concentration of approximately 400 mM (411 mM), as shown in Figure 8. The initial positions of the drug molecules are completely randomly distributed on both sides of the membrane. We find that the drug forms long chains of drug molecules above the membrane surface that gradually push down and permeate the bilayer after approximately 1 μs shown in Figure 8B. A fraction of these drug population breaks off and remain in the bilayer, while the rest of the long chains form a filament above the membrane surface at 1.8 Figure 8C. These long chains locally distort the interfacial concentration of the POPC chains. In Supporting Figure 14, the electron density profile shows the CPT molecules distributed randomly in solution above the membrane about 40 Å away from the COM of the POPC bilayer. As shown, after 1.6 μs, the CPT peak on the electron density profile becomes sharper and shifts 50−65 Å away from the COM of the POPC bilayer (location of filament), with a secondary peak due to drugs that break off and insert themselves into the hydrophobic membrane just under the POPC headgroups.

The sharper peak of CPT in Supporting Figure 14 is due to well-organized CPT−CPT stacking. As Kang et al. suggests, a dominant feature of CPT in solution is $\pi-\pi$ stacking.[48] With this highly concentrated system, the CPT−CPT stacking via $\pi-\pi$ interactions greatly impacts CPT orientation and also its permeation pathway into the membrane. Hence, it is interesting to compare the orientation of multiple CPTs interacting with the membrane against the singular CPT system. We calculate the θ angles between every CPT and the membrane normal vector, as shown in Supporting Figure 2. Interestingly, with the CPT−CPT stacking the violin plot of θ angles shifts its shape significantly from the singular CPT θ angle. In Supporting Figure 15, contrary to expectation where CPTs should rotate freely at 50−65 Å away from the COM of the POPC bilayer, the higher concentration of CPTs is given by three populations that correspond to three orientations of CPTs with respect to the membrane normal vector: parallel (~6°), perpendicular (~75°−100°), and antiparallel (~175°). These three orientations are caused by pronounced CPT−CPT stacking and are absent in the singular CPT systems. To test if the formation of filamentous assemblies is dependent on the initial concentration of the drug, we next ran three additional concentrations. All simulation runs of varying CPT concentration above the membrane are summarized in Supporting Table 1. We ran two additional high concentration systems at 24 and 94 mM. In addition, one additional replica containing a single CPT was run, to test passive diffusion for one drug only. All three systems at high concentrations (24, 94, and 411 mM) show the formation of filamentous assemblies. The additional replica containing a single CPT the drug enters the membrane after 16 ns. The electron density over time, as well as the order parameter of the phospholipid tails, is shown in Supporting Figures 16−19. We note that the trend in these systems is that the drugs penetrate into the membrane in groups of 2−3, but longer chains of drugs do not insert. Thus, the presence of additional surrounding drugs greatly modifies the orientation of each CPT with the membrane as the drugs form stacks that lay on top of the phospholipid bilayer but do not directly interact. We note that the formation of the drugs into these long stacks above the membrane effectively reduce the rotational entropy of the drug, shifting its contribution to the free energy profile across the bilayer and greatly affect the membrane permeation pathway. In addition, the hydroxyl group of the CPT cannot easily form H bonds with the membrane surface. In comparison with experiments, the experimentally reported partition coefficients from Selvi et al.[74] are at the 0.11 μg/mL or around approximately 30 μM concentration. Furthermore,

https://dx.doi.org/10.1021/acs.jctc.9b00541
J. Chem. Theory Comput. XXXX, XXX, XXX−XXX

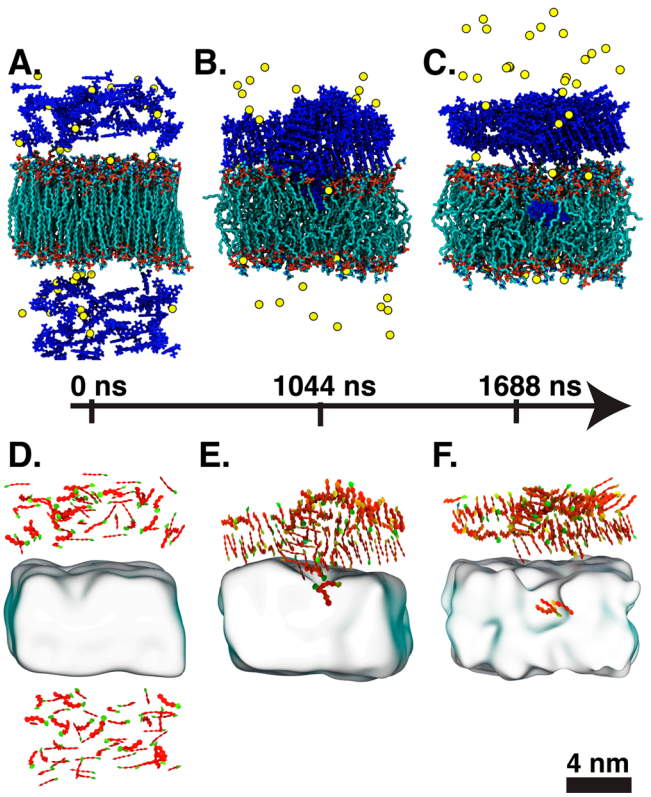

Figure 8. (A) Snapshot of the CPTs at high concentration, starting configuration at 0 μs. POPC is shown in Licorice representation. CPT is shown in blue. (B) A snapshot of the CPTs at high concentration ordering above the membrane, after starting to insert into the POPC bilayer at 1.044 μs. The drug forms stacks along the surface of the membrane. Several drugs start to insert just under the phospholipid headgroups. POPC is shown in Licorice representation. (C) CPTs above the membrane with few remaining CPTs inside the membrane at 1.68 μs CPT. (D, E) CPT is shown in Paperchain presentation and the POPC is shown as a transparent slab. The drug forms stacks along the surface of the membrane. Several drugs start to insert just under the phospholipid headgroups.

the experimental concentrations by Cheetham et al.[49] are in the 50 μM range; however, supramolecular aggregates, as reported by Cheetham et al.,[49] expect that a high concentration of CPTs are stable in supramolecular aggregate form at 20 μM. While the lowest concentration we simulate is ∼4 mM is 50 nearly times more concentrated than this concentration, the local concentration of CPT's may be increased if interactions with the membrane destabilize individual supramolecular aggregates. Effectively, the membrane may serve as a surface that is nucleating and growing unidimensional drug crystals. The membrane itself may lower the critical concentration for growth of these supramolecular aggregates.

5. CONCLUSION

We summarize the results of the calculated partition coefficient for the three model systems as calculated with the adaptive biasing force (ABF) methodology in Table 2. In comparison with experimentally reported partition coefficients, the value for log $P_{octanol/water}$ that we calculate from the transfer free energy are off by a factor of 2. However, calculation via the second methodology, from integration over the potential of mean force, gives a closer agreement (2.2) with the experimentally reported value (1.74). Surprising, calculation of the partition coefficient using the second methodology, integrating over a thin octanol bilayer gives excellent agreement (1.8) with experimental partition coefficient (1.74[72]). For the POPC membrane, we find that the value of the partition coefficient calculated from the transfer free energy (4.1) is extremely high compared to the experimentally reported value for a model DOPC membrane (1.65[74]). However, recalculation via the second methodology (1.9) gives closer agreement. The closer agreement of the calculated partition coefficient, log K, with experimentally reported values for the partition efficient implies that interfacial structure plays a critical role in all three interfaces. Indeed, the minima in the PMFs for the first and third interface are 5 Å or less from the thickness of the interface as defined by the density profile. For the second interface, the minimum in the PMF is ∼20 Å from the bulk octanol surface. Therefore, in all three cases, one can infer that the drug will be interfacially active, with more drug partitioning close to the interface, as opposed to the bulk.

We note that the lack of polarization in the TIP3P water model may provide the wrong baseline for partitioning and the lack of polarization may impact transfer free energies. While force fields that include polarizability may lead to higher accuracy for the transfer free energies, this would come at an increased computational cost. Including polarizability of the water, or else the phospholipids, could impact the permeation pathways.[76,77] Herein, we attempt to correlate the strength of hydrogen bonding of this model hydrophobic cancer drug, CPT, with a model phospholipid bilayer with the rotational entropy of the drug. We show that the two are inversely correlated, with an anticorrelation coefficient of −0.47. In particular, the orientation of the drug with respect to each model interface is determined to some degree due to the strength of hydrogen bonding at each respective interface. Most notably, because of the planar pentacyclic structure of CPT, it can form strong aromatic interactions with itself. We show that these strong aromatic interactions lead to the formation of stacks of drug that form across the membrane at higher concentrations. The formation of CPT drug stacks modulates the interaction of the drug with the phospholipid bilayer, shifting the orientation of the drug with respect to the membrane, changing the membrane permeation pathway.

Table 2. $\Delta G_{barrier}$, $\Delta G_{transfer}$, and Partition Coefficients (log P and log K) as Defined in the Methods Section Based on Average over All Replicas for Each Interface[a]

	simulations				experiments
	$\Delta G_{barrier}$ (kcal/mol)	$\Delta G_{transfer}$(kcal/mol)	log P	log K	log P (experimental)
octanol bilayer (interface I)	0.27 ± 0.15	5.5	4.0	1.8	N/A
thick octanol layer (interface II)	N/A	6.2	4.6	2.2	1.74[72]
POPC membrane bilayer (interface III)	3.8 ± 0.8	5.8	4.1	1.9	1.65 (with DOPC)[74]

[a]Comparison with experimentally reported partition coefficients from refs 72 and 74.

https://dx.doi.org/10.1021/acs.jctc.9b00541
J. Chem. Theory Comput. XXXX, XXX, XXX−XXX

With the increasing computational power available, in addition to recent increasing interest in the power of machine learning approaches to predict small drug permeability in membranes,[12−14] we note that further characterization of variables and/or hidden reaction coordinates that determine small drug permeability in membranes is urgent.[78,79] However, we note that these models have so far not accounted for the strength of drug−drug interactions on the modulation of the permeability into the membrane. This may be an additional consideration that needs to be taken into account into these models. A methodology uniquely suitable for exploring the contribution of drug−drug interactions on membrane permeability is rational coarse-grained methods.[79,80]

■ ASSOCIATED CONTENT

Supporting Information

The Supporting Information is available free of charge at https://pubs.acs.org/doi/10.1021/acs.jctc.9b00541.

Summary of additional simulation runs at varying CPT concentrations above the membrane, the structure of CPT, schematic illustration of the angle between the membrane and normal vector, additional snapshots and electron densities for the three interfaces, the time evolution of the PMF profiles for all three interfaces, time-dependent plots of orientation angles, hydrogen bonds, rotational entropy, thermodynamic contributions and matrixes of cross correlation coefficients, and the electron density profiles and order parameters of the POPC tails for the high concentration CPT systems are also characterized (PDF)

■ AUTHOR INFORMATION

Corresponding Author

Sharon M. Loverde − *Department of Chemistry, College of Staten Island and Department of Physics, Graduate Center, City University of New York, Staten Island, New York 10314, United States; Ph.D. Program in Chemistry, Biochemistry, and Physics, The Graduate Center of the City University of New York, New York, New York 10016, United States;* orcid.org/0000-0002-7643-6498; Phone: 718-982-4075; Email: sharon.loverde@csi.cuny.edu

Authors

Phu K. Tang − *Ph.D. Program in Chemistry, Biochemistry, and Physics, The Graduate Center of the City University of New York, New York, New York 10016, United States; Department of Chemistry, College of Staten Island, City University of New York, Staten Island, New York 10314, United States*

Kaushik Chakraborty − *Department of Chemistry, College of Staten Island, City University of New York, Staten Island, New York 10314, United States*

William Hu − *Department of Chemistry, College of Staten Island, City University of New York, Staten Island, New York 10314, United States*

Myungshim Kang − *Department of Chemistry, College of Staten Island, City University of New York, Staten Island, New York 10314, United States*

Complete contact information is available at: https://pubs.acs.org/10.1021/acs.jctc.9b00541

Author Contributions

[⊥]K.C. and W.H. are co-second authors.

Notes

The authors declare no competing financial interest.

■ ACKNOWLEDGMENTS

This research was supported, in part, by the NSF through XSEDE resources under Grant CHE130099 and a grant of computer time from the City University of New York High Performance Computing Center under NSF Grants CNS-0855217, CNS-0958379, and ACI-1126113. S.M.L. acknowledges start-up funding received from College of Staten Island and City University of New York. S.M.L. would also like to acknowledge NSF Grant DMR-1750694 and support from the NIH (R15EB020343-01A1).

■ REFERENCES

(1) PhRMA. *Pharmaceutical Industry Profile*, 2018. http://phrmadocs.phrma.org/industryprofile/2018/pdfs/2018_IndustryProfile_Brochure.pdf.

(2) Kola, I.; Landis, J. Can the Pharmaceutical Industry Reduce Attrition Rates? *Nat. Rev. Drug Discovery* **2004**, *3* (8), 711−5.

(3) Arrowsmith, J. Trial Watch: Phase Ii Failures: 2008−2010. *Nat. Rev. Drug Discovery* **2011**, *10* (5), 328−9.

(4) Arrowsmith, J. Trial Watch: Phase Iii and Submission Failures: 2007−2010. *Nat. Rev. Drug Discovery* **2011**, *10* (2), 87.

(5) Munos, B. Lessons from 60 Years of Pharmaceutical Innovation. *Nat. Rev. Drug Discovery* **2009**, *8* (12), 959−68.

(6) Missner, A.; Pohl, P. 110 Years of the Meyer-Overton Rule: Predicting Membrane Permeability of Gases and Other Small Compounds. *ChemPhysChem* **2009**, *10* (9−10), 1405−14.

(7) Alves de Lima Ribeiro, F.; Ferreira, M. M. C. Qspr Models of Boiling Point, Octanol−Water Partition Coefficient and Retention Time Index of Polycyclic Aromatic Hydrocarbons. *J. Mol. Struct.: THEOCHEM* **2003**, *663* (1−3), 109−126.

(8) Hopfinger, A. J.; Wang, S.; Tokarski, J. S.; Jin, B.; Albuquerque, M.; Madhav, P. J.; Duraiswami, C. Construction of 3d-Qsar Models Using the 4d-Qsar Analysis Formalism. *J. Am. Chem. Soc.* **1997**, *119* (43), 10509−10524.

(9) Yoshida, F.; Topliss, J. G. Qsar Model for Drug Human Oral Bioavailability. *J. Med. Chem.* **2000**, *43* (13), 2575−85.

(10) Zhao, Y. H.; Le, J.; Abraham, M. H.; Hersey, A.; Eddershaw, P. J.; Luscombe, C. N.; Butina, D.; Beck, G.; Sherborne, B.; Cooper, I.; Platts, J. A. Erratum: Evaluation of Human Intestinal Absorption Data and Subsequent Derivation of a Quantitative Structure−Activity Relationship (Qsar) with the Abraham Descriptors. *J. Pharm. Sci.* **2002**, *91* (2), 605.

(11) Zhang, L.; Zhu, H.; Oprea, T. I.; Golbraikh, A.; Tropsha, A. Qsar Modeling of the Blood-Brain Barrier Permeability for Diverse Organic Compounds. *Pharm. Res.* **2008**, *25* (8), 1902−14.

(12) Brocke, S. A.; Degen, A.; MacKerell, A. D.; Dutagaci, B.; Feig, M. Prediction of Membrane Permeation of Drug Molecules by Combining an Implicit Membrane Model with Machine Learning. *J. Chem. Inf. Model.* **2019**, *59* (3), 1147−1162.

(13) Menichetti, R.; Kanekal, K. H.; Bereau, T. Drug-Membrane Permeability across Chemical Space. *ACS Cent. Sci.* **2019**, *5* (2), 290−298.

(14) Menichetti, R.; Kanekal, K. H.; Bereau, T. Investigating Drug-Membrane Permeability across Chemical Compound Space Using High-Throughput Coarse-Grained Simulations. *Biophys. J.* **2019**, *116* (3), 318A−318A.

(15) Parisio, G.; Stocchero, M.; Ferrarini, A. Passive Membrane Permeability: Beyond the Standard Solubility-Diffusion Model. *J. Chem. Theory Comput.* **2013**, *9* (12), 5236−5246.

(16) Finkelstein, A. Water and Nonelectrolyte Permeability of Lipid Bilayer Membranes. *J. Gen. Physiol.* **1976**, *68* (2), 127−135.

(17) Jambeck, J. P. M.; Lyubartsev, A. P. Exploring the Free Energy Landscape of Solutes Embedded in Lipid Bilayers. *J. Phys. Chem. Lett.* **2013**, *4* (11), 1781−1787.

(18) Comer, J.; Schulten, K.; Chipot, C. Diffusive Models of Membrane Permeation with Explicit Orientational Freedom. *J. Chem. Theory Comput.* **2014**, *10* (7), 2710−8.
(19) Bonhenry, D.; Tarek, M.; Dehez, F. Effects of Phospholipid Composition on the Transfer of a Small Cationic Peptide across a Model Biological Membrane. *J. Chem. Theory Comput.* **2013**, *9* (12), 5675−84.
(20) Tse, C. H.; Comer, J.; Sang Chu, S. K.; Wang, Y.; Chipot, C. Affordable Membrane Permeability Calculations: Permeation of Short-Chain Alcohols through Pure-Lipid Bilayers and a Mammalian Cell Membrane. *J. Chem. Theory Comput.* **2019**, *15* (5), 2913−2924.
(21) Tse, C. H.; Comer, J.; Wang, Y.; Chipot, C. Link between Membrane Composition and Permeability to Drugs. *J. Chem. Theory Comput.* **2018**, *14* (6), 2895−2909.
(22) Klein, M. L.; Shinoda, W. Large-Scale Molecular Dynamics Simulations of Self-Assembling Systems. *Science* **2008**, *321* (5890), 798−800.
(23) Kang, M.; Cui, H.; Loverde, S. M. Coarse-Grained Molecular Dynamics Studies of the Structure and Stability of Peptide-Based Drug Amphiphile Filaments. *Soft Matter* **2017**, *13* (42), 7721−7730.
(24) Mayor, U.; Johnson, C. M.; Daggett, V.; Fersht, A. R. Protein Folding and Unfolding in Microseconds to Nanoseconds by Experiment and Simulation. *Proc. Natl. Acad. Sci. U. S. A.* **2000**, *97* (25), 13518−22.
(25) Mayor, U.; Guydosh, N. R.; Johnson, C. M.; Grossmann, J. G.; Sato, S.; Jas, G. S.; Freund, S. M.; Alonso, D. O.; Daggett, V.; Fersht, A. R. The Complete Folding Pathway of a Protein from Nanoseconds to Microseconds. *Nature* **2003**, *421* (6925), 863−7.
(26) Zomot, E.; Gur, M.; Bahar, I. Microseconds Simulations Reveal a New Sodium-Binding Site and the Mechanism of Sodium-Coupled Substrate Uptake by Leut. *J. Biol. Chem.* **2015**, *290* (1), 544−55.
(27) Roux, B. The Calculation of the Potential of Mean Force Using Computer Simulations. *Comput. Phys. Commun.* **1995**, *91* (1−3), 275−282.
(28) Domenech, O.; Francius, G.; Tulkens, P. M.; Van Bambeke, F.; Dufrene, Y.; Mingeot-Leclercq, M. P. Interactions of Oritavancin, a New Lipoglycopeptide Derived from Vancomycin, with Phospholipid Bilayers: Effect on Membrane Permeability and Nanoscale Lipid Membrane Organization. *Biochim. Biophys. Acta, Biomembr.* **2009**, *1788* (9), 1832−40.
(29) Genheden, S.; Essex, J. W. A Simple and Transferable All-Atom/Coarse-Grained Hybrid Model to Study Membrane Processes. *J. Chem. Theory Comput.* **2015**, *11* (10), 4749−59.
(30) Lee, C. T.; Comer, J.; Herndon, C.; Leung, N.; Pavlova, A.; Swift, R. V.; Tung, C.; Rowley, C. N.; Amaro, R. E.; Chipot, C.; Wang, Y.; Gumbart, J. C. Simulation-Based Approaches for Determining Membrane Permeability of Small Compounds. *J. Chem. Inf. Model.* **2016**, *56* (4), 721−33.
(31) Comer, J.; Schulten, K.; Chipot, C. Calculation of Lipid-Bilayer Permeabilities Using an Average Force. *J. Chem. Theory Comput.* **2014**, *10* (2), 554−64.
(32) Comer, J.; Schulten, K.; Chipot, C. Permeability of a Fluid Lipid Bilayer to Short-Chain Alcohols from First Principles. *J. Chem. Theory Comput.* **2017**, *13* (6), 2523−2532.
(33) Kirkwood, J. G. Statistical Mechanics of Fluid Mixtures. *J. Chem. Phys.* **1935**, *3* (5), 300−313.
(34) Straatsma, T. P.; McCammon, J. A. Multiconfiguration Thermodynamic Integration. *J. Chem. Phys.* **1991**, *95* (2), 1175−1188.
(35) Laio, A.; Parrinello, M. Escaping Free-Energy Minima. *Proc. Natl. Acad. Sci. U. S. A.* **2002**, *99* (20), 12562−6.
(36) Barducci, A.; Bussi, G.; Parrinello, M. Well-Tempered Metadynamics: A Smoothly Converging and Tunable Free-Energy Method. *Phys. Rev. Lett.* **2008**, *100* (2), No. 020603.
(37) Ghaemi, Z.; Alberga, D.; Carloni, P.; Laio, A.; Lattanzi, G. Permeability Coefficients of Lipophilic Compounds Estimated by Computer Simulations. *J. Chem. Theory Comput.* **2016**, *12* (8), 4093−9.
(38) Sun, R.; Dama, J. F.; Tan, J. S.; Rose, J. P.; Voth, G. A. Transition-Tempered Metadynamics Is a Promising Tool for Studying the Permeation of Drug-Like Molecules through Membranes. *J. Chem. Theory Comput.* **2016**, *12* (10), 5157−5169.
(39) Kumar, S.; Rosenberg, J. M.; Bouzida, D.; Swendsen, R. H.; Kollman, P. A. The Weighted Histogram Analysis Method for Free-Energy Calculations on Biomolecules. I. The Method. *J. Comput. Chem.* **1992**, *13* (8), 1011−1021.
(40) Henin, J.; Chipot, C. Overcoming Free Energy Barriers Using Unconstrained Molecular Dynamics Simulations. *J. Chem. Phys.* **2004**, *121* (7), 2904−14.
(41) Darve, E.; Rodriguez-Gomez, D.; Pohorille, A. Adaptive Biasing Force Method for Scalar and Vector Free Energy Calculations. *J. Chem. Phys.* **2008**, *128* (14), 144120.
(42) Bhatnagar, N.; Kamath, G.; Chelst, I.; Potoff, J. J. Direct Calculation of 1-Octanol−Water Partition Coefficients from Adaptive Biasing Force Molecular Dynamics Simulations. *J. Chem. Phys.* **2012**, *137* (1), 014502.
(43) Comer, J.; Gumbart, J. C.; Henin, J.; Lelievre, T.; Pohorille, A.; Chipot, C. The Adaptive Biasing Force Method: Everything You Always Wanted to Know but Were Afraid to Ask. *J. Phys. Chem. B* **2015**, *119* (3), 1129−51.
(44) Wall, M. E.; Wani, M. C.; Cook, C. E.; Palmer, K. H.; McPhail, A. T.; Sim, G. A. Plant Antitumor Agents. I. The Isolation and Structure of Camptothecin, a Novel Alkaloidal Leukemia and Tumor Inhibitor from Camptotheca Acuminata1,2. *J. Am. Chem. Soc.* **1966**, *88* (16), 3888−3890.
(45) Minko, T.; Paranjpe, P. V.; Qiu, B.; Lalloo, A.; Won, R.; Stein, S.; Sinko, P. J. Enhancing the Anticancer Efficacy of Camptothecin Using Biotinylated Poly(Ethylene Glycol) Conjugates in Sensitive and Multidrug-Resistant Human Ovarian Carcinoma Cells. *Cancer Chemother. Pharmacol.* **2002**, *50* (2), 143−50.
(46) Staker, B. L.; Hjerrild, K.; Feese, M. D.; Behnke, C. A.; Burgin, A. B., Jr.; Stewart, L. The Mechanism of Topoisomerase I Poisoning by a Camptothecin Analog. *Proc. Natl. Acad. Sci. U. S. A.* **2002**, *99* (24), 15387−92.
(47) Yue, Z.; Li, C. H.; Voth, G. A.; Swanson, J. M. J. Dynamic Protonation Dramatically Affects the Membrane Permeability of Drug-Like Molecules. *J. Am. Chem. Soc.* **2019**, *141* (34), 13421−13433.
(48) Kang, M.; Zhang, P.; Cui, H.; Loverde, S. M. Pi-Pi Stacking Mediated Chirality in Functional Supramolecular Filaments. *Macromolecules* **2016**, *49* (3), 994−1001.
(49) Cheetham, A. G.; Zhang, P. C.; Lin, Y. A.; Lock, L. L.; Cui, H. G. Supramolecular Nanostructures Formed by Anticancer Drug Assembly. *J. Am. Chem. Soc.* **2013**, *135* (8), 2907−2910.
(50) Schlitter, J. Estimation of Absolute and Relative Entropies of Macromolecules Using the Covariance-Matrix. *Chem. Phys. Lett.* **1993**, *215* (6), 617−621.
(51) Chakraborty, K.; Khatua, P.; Bandyopadhyay, S. Exploring Ion Induced Folding of a Single-Stranded DNA Oligomer from Molecular Simulation Studies. *Phys. Chem. Chem. Phys.* **2016**, *18* (23), 15899−910.
(52) Chakraborty, K.; Sinha, S. K.; Bandyopadhyay, S. Thermodynamics of Complex Structures Formed between Single-Stranded DNA Oligomers and the Kh Domains of the Far Upstream Element Binding Protein. *J. Chem. Phys.* **2016**, *144* (20), 205105.
(53) Martinez, L.; Andrade, R.; Birgin, E. G.; Martinez, J. M. Packmol: A Package for Building Initial Configurations for Molecular Dynamics Simulations. *J. Comput. Chem.* **2009**, *30* (13), 2157−64.
(54) Vanommeslaeghe, K.; Hatcher, E.; Acharya, C.; Kundu, S.; Zhong, S.; Shim, J.; Darian, E.; Guvench, O.; Lopes, P.; Vorobyov, I.; Mackerell, A. D., Jr. Charmm General Force Field: A Force Field for Drug-Like Molecules Compatible with the Charmm All-Atom Additive Biological Force Fields. *J. Comput. Chem.* **2009**, *31* (4), 671−90.
(55) Klauda, J. B.; Venable, R. M.; Freites, J. A.; O'Connor, J. W.; Tobias, D. J.; Mondragon-Ramirez, C.; Vorobyov, I.; MacKerell, A. D., Jr.; Pastor, R. W. Update of the Charmm All-Atom Additive Force

https://dx.doi.org/10.1021/acs.jctc.9b00541
J. Chem. Theory Comput. XXXX, XXX, XXX−XXX

Field for Lipids: Validation on Six Lipid Types. *J. Phys. Chem. B* **2010**, *114* (23), 7830−43.
(56) Lee, S.; Tran, A.; Allsopp, M.; Lim, J. B.; Henin, J.; Klauda, J. B. Charmm36 United Atom Chain Model for Lipids and Surfactants. *J. Phys. Chem. B* **2014**, *118* (2), 547−56.
(57) Vanommeslaeghe, K.; MacKerell, A. D., Jr. Charmm Additive and Polarizable Force Fields for Biophysics and Computer-Aided Drug Design. *Biochim. Biophys. Acta, Gen. Subj.* **2015**, *1850* (5), 861−871.
(58) Huang, L.; Roux, B. Automated Force Field Parameterization for Non-Polarizable and Polarizable Atomic Models Based on Ab Initio Target Data. *J. Chem. Theory Comput.* **2013**, *9* (8), 3543.
(59) Kucerka, N.; Nieh, M. P.; Katsaras, J. Fluid Phase Lipid Areas and Bilayer Thicknesses of Commonly Used Phosphatidylcholines as a Function of Temperature. *Biochim. Biophys. Acta, Biomembr.* **2011**, *1808* (11), 2761−71.
(60) Phillips, J. C.; Braun, R.; Wang, W.; Gumbart, J.; Tajkhorshid, E.; Villa, E.; Chipot, C.; Skeel, R. D.; Kale, L.; Schulten, K. Scalable Molecular Dynamics with Namd. *J. Comput. Chem.* **2005**, *26* (16), 1781−802.
(61) Martyna, G. J.; Tobias, D. J.; Klein, M. L. Constant Pressure Molecular Dynamics Algorithms. *J. Chem. Phys.* **1994**, *101* (5), 4177−4189.
(62) Feller, S. E.; Zhang, Y.; Pastor, R. W.; Brooks, B. R. Constant Pressure Molecular Dynamics Simulation: The Langevin Piston Method. *J. Chem. Phys.* **1995**, *103* (11), 4613−4621.
(63) Andersen, H. C. Rattle: A "Velocity" Version of the Shake Algorithm for Molecular Dynamics Calculations. *J. Comput. Phys.* **1983**, *52* (1), 24−34.
(64) Darden, T.; York, D.; Pedersen, L. Particle Mesh Ewald: An N·Log(N) Method for Ewald Sums in Large Systems. *J. Chem. Phys.* **1993**, *98* (12), 10089−10092.
(65) Rodriguez-Gomez, D.; Darve, E.; Pohorille, A. Assessing the Efficiency of Free Energy Calculation Methods. *J. Chem. Phys.* **2004**, *120* (8), 3563−78.
(66) Straatsma, T. P.; Berendsen, H. J. C.; Stam, A. J. Estimation of Statistical Errors in Molecular Simulation Calculations. *Mol. Phys.* **1986**, *57* (1), 89−95.
(67) Isralewitz, B.; Baudry, J.; Gullingsrud, J.; Kosztin, D.; Schulten, K. Steered Molecular Dynamics Investigations of Protein Function. *J. Mol. Graphics Modell.* **2001**, *19* (1), 13−25.
(68) Paloncyova, M.; DeVane, R.; Murch, B.; Berka, K.; Otyepka, M. Amphiphilic Drug-Like Molecules Accumulate in a Membrane Below the Head Group Region. *J. Phys. Chem. B* **2014**, *118* (4), 1030−1039.
(69) Carlsson, J.; Aqvist, J. Absolute and Relative Entropies from Computer Simulation with Applications to Ligand Binding. *J. Phys. Chem. B* **2005**, *109* (13), 6448−6456.
(70) McNaught, A. D.; Wilkinson, A. *IUPAC Compendium of Chemical Terminology*, 2nd ed., The Gold Book; Blackwell Scientific Publications: Oxford, 1997.
(71) Roe, D. R.; Cheatham, T. E., 3rd Ptraj and Cpptraj: Software for Processing and Analysis of Molecular Dynamics Trajectory Data. *J. Chem. Theory Comput.* **2013**, *9* (7), 3084−95.
(72) Leo, A.; Hansch, C.; Elkins, D. Partition Coefficients and Their Uses. *Chem. Rev.* **1971**, *71* (6), 525−616.
(73) MacCallum, J. L.; Tieleman, D. P. Structures of Neat and Hydrated 1-Octanol from Computer Simulations. *J. Am. Chem. Soc.* **2002**, *124* (50), 15085−93.
(74) Selvi, B.; Patel, S.; Savva, M. Physicochemical Characterization and Membrane Binding Properties of Camptothecin. *J. Pharm. Sci.* **2008**, *97* (10), 4379−90.
(75) Kang, M.; Loverde, S. M. Molecular Simulation of the Concentration-Dependent Interaction of Hydrophobic Drugs with Model Cellular Membranes. *J. Phys. Chem. B* **2014**, *118* (41), 11965−72.
(76) Kramer, A.; Pickard, F. C.; Huang, J.; Venable, R. M.; Simmonett, A. C.; Reith, D.; Kirschner, K. N.; Pastor, R. W.; Brooks, B. R. Interactions of Water and Alkanes: Modifying Additive Force Fields to Account for Polarization Effects. *J. Chem. Theory Comput.* **2019**, *15* (6), 3854−3867.
(77) Venable, R. M.; Kramer, A.; Pastor, R. W. Molecular Dynamics Simulations of Membrane Permeability. *Chem. Rev.* **2019**, *119* (9), 5954−5997.
(78) Shinoda, W. Permeability across Lipid Membranes. *Biochim. Biophys. Acta, Biomembr.* **2016**, *1858* (10), 2254−2265.
(79) Loverde, S. M. Molecular Simulation of the Transport of Drugs across Model Membranes. *J. Phys. Chem. Lett.* **2014**, *5* (10), 1659−65.
(80) Loverde, S. M.; Klein, M. L.; Discher, D. E. Nanoparticle Shape Improves Delivery: Rational Coarse Grain Molecular Dynamics (Rcg-Md) of Taxol in Worm-Like Peg-Pcl Micelles. *Adv. Mater.* **2012**, *24* (28), 3823−3830.

https://dx.doi.org/10.1021/acs.jctc.9b00541
J. Chem. Theory Comput. XXXX, XXX, XXX−XXX